

Simultaneous acquisition of high-contrast and quantitative liver T1 images using 3D phase-sensitive inversion recovery: A feasibility study

メタデータ	言語: eng 出版者: 公開日: 2018-05-24 キーワード (Ja): キーワード (En): 作成者: Fujiwara, Yasuhiro, Maruyama, Hirotoshi, Kosaka, Nobuyuki, Ishimori, Yoshiyuki メールアドレス: 所属:
URL	http://hdl.handle.net/10098/10431

TITLE

Simultaneous acquisition of high-contrast and quantitative liver T_1 images using 3D phase-sensitive inversion recovery: A feasibility study

Yasuhiro Fujiwara¹, Hirotohi Maruyama², Nobuyuki Kosaka³, Yoshiyuki Ishimori⁴

1) Department of Medical Imaging, Faculty of Life Sciences, Kumamoto University

2) Radiological Center, National Hospital Organization Kumamoto Medical Center

3) Department of Radiology, University of Fukui

4) Department of Radiological Sciences, Ibaraki Prefectural University of Health Sciences

Corresponding author: Yasuhiro Fujiwara, PhD.

Department of Medical Imaging, Faculty of Life Sciences, Kumamoto University

4-24-1 Kuhonji, Chuo-ku, Kumamoto, Japan

Phone: +81-96-373-5454; Fax: +81-96-373-5454; E-mail: yfuji@kumamoto-u.ac.jp

Abstract

Background: Tumor-to-liver contrast is low in images of chronically diseased livers because gadolinium-based hepatocyte-specific contrast agents (Gd-EOB-DTPA) accumulate less to hepatocytes.

Purpose: To determine whether phase-sensitive inversion recovery (PSIR) could improve the T_1 contrasts of Gd-based contrast agents and liver parenchyma and simultaneously provide accurate T_1 values for abdominal organs.

Material and Methods: The image contrasts of phantoms with different Gd concentrations that were obtained using PSIR were compared to conventional turbo field echo (TFE) results. T_1 value was estimated using PSIR by performing iterations to investigate the two IR magnetization evolutions. The estimated T_1 values were validated using IR-spin echo (IR-SE) and Look-Locker (L-L) sequences. In an *in vivo* study, the liver-to-spleen and liver-to-muscle contrasts of the PSIR and TFE images of seven volunteers were compared, as were the T_1 values of liver parenchyma, spleen, and muscle obtained using PSIR and L-L sequences.

Results: The PSIR images showed T_1 contrasts higher than those in the TFE results. The PSIR and IR-SE T_1 values were linearly correlated. Additionally, the R_1 estimated using PSIR were correlated with those measured using IR-SE and L-L. In the *in vivo* study, the liver-to-spleen and liver-to-muscle contrasts of PSIR were significantly higher than those obtained using TFE. T_1 values of abdominal organs obtained using PSIR and L-L were clearly correlated.

Conclusion: PSIR may be capable of improving liver image T_1 contrasts when Gd-based contrast agents are employed and simultaneously yielding accurate T_1 values of abdominal organs.

Keywords: magnetic resonance imaging (MRI), liver imaging, phase-sensitive inversion recovery (PSIR), quantitative MRI, T_1 mapping

Introduction

Gadolinium ethoxybenzyl diethylenetriamine pentaacetic acid (Gd-EOB-DTPA) has been widely used for liver MRI to detect liver tumors. Gd-EOB-DTPA differs from conventional Gd-based contrast agents because it enables not only tumor vascularity assessment during dynamic-contrast-enhanced imaging, but also liver tumor detection due to the high T_1 contrast between a tumor and the surrounding liver parenchyma in the hepatobiliary phase. This excellent tumor-to-liver contrast is established by the high uptake of Gd-EOB-DTPA by hepatocyte (1). However, liver parenchyma accumulation is lower in patients with chronic liver diseases, which may cause liver lesions to be missed (2, 3). Thus, improvement of the T_1 contrast between a tumor and the liver parenchyma in the hepatobiliary phase would be advantageous for liver MRI using Gd-EOB-DTPA (EOB-MRI). However, reports on T_1 contrast improvement have been limited so far. A few clinical studies have shown that increasing the flip angle (FA) in the hepatobiliary phase improves the detection rates and conspicuousness of a wide spectrum of hypointense lesions (4–8). However, using a higher FA causes a higher specific absorption rate and inhomogeneous fat suppression, which are drawbacks for clinical liver imaging.

More recently, it was found that Gd-EOB-DTPA accumulation in patients with damaged liver parenchyma decreased with decreasing liver function (9). By quantifying the Gd-EOB-DTPA accumulation in liver parenchyma, EOB-MRI can also be used to assess liver fibrosis or reserve in chronic liver diseases (9–17). Moreover, T_1 value has also been useful for differential diagnosis of liver tumors (18). Thus, multi-slice acquisition covering the entire liver with higher spatial resolution is desirable for liver T_1 mapping. However, since the number of slices that may be acquired is limited, and thus the entire liver area cannot be

imaged simultaneously, conventional T_1 measurement methods such as the Look-Locker (L-L) are insufficient for this purpose (19, 20).

In this study, we applied 3D phase-sensitive inversion recovery (PSIR) for liver imaging. Since such sequences have been successfully used for cardiac MRI to improve late Gd-DTPA enhancement in cardiac muscles (21), they were expected to enable tumor-to-liver T_1 contrast improvement. Moreover, these sequences can simultaneously provide quantitative T_1 maps of the entire liver without requiring any additional scans (22). Our objective was to determine whether PSIR could improve the T_1 contrasts of Gd-based contrast agents and liver parenchyma and thus simultaneously provide accurate T_1 values for abdominal organs. For this purpose, we compared the T_1 contrasts and T_1 values of images of phantoms with different Gd concentrations as well as *in vivo* images of abdominal organs obtained by different sequences including PSIR to demonstrate the utility of PSIR for liver MR imaging.

Material and Methods

Phantom study

MRI was performed with a 3.0 T clinical MRI system with a 32-channel phased-array body receive coil (Ingenia, Philips Healthcare, Best, The Netherlands). PSIR was performed using an inversion recovery turbo field echo (IR-TFE) readout. Fig. 1 shows the magnetization evolution during PSIR acquisition. By acquiring an additional TFE after obtaining the IR-TFE, PSIR was used to remove the background phase while preserving the sign of the desired magnetization for phase correction (21).

From the relationships between the two IR magnetization evolutions, the fully relaxed magnetization and T_1 values were calculated, as described by Warntjes et al. (22). The magnetization (M_A) after the applying the IR pulse evolves by T_1 during the inversion time (TI). After TI, RF pulses are applied each repetition time (TR) to excite M_B during the

acquisition time (T_{acq}) and thereby to obtain the first magnetization signal. M_B relaxes by T_1^* towards a saturated magnetization (M_0^*). T_1^* and M_0^* can be obtained using

$$\frac{M_0^*}{M_0} = \frac{T_1^*}{T_1} = \frac{TR}{TR - T_1 \ln(\cos\alpha)}, \quad (1)$$

where α is the FA. After the first acquisition, the magnetization evolves by T_1 . Then, following the time shot interval from the IR pulse and TI, a second magnetization to obtain reference data is acquired from M_D to M_E . After the second acquisition, the magnetization relaxes by T_1 from M_E to M_F . M_B and M_C can be expressed as

$$M_B = M_0 - (M_0 - M_A) \exp\left(-\frac{TI}{T_1}\right) \quad (2)$$

and

$$M_C = M_0^* - (M_0^* - M_B) \exp\left(-\frac{T_{acq}}{T_1^*}\right). \quad (3)$$

M_D and M_F can be obtained using equations similar to Eq. 2, while M_E can be determined using an equation similar to Eq. 3. The T_1 values were calculated by applying these equations iteratively.

Twelve phantoms containing 1.0% agarose solution and different concentrations (0.04, 0.08, 0.10, 0.16, 0.20, 0.30, 0.40, 0.50, 0.60, 0.75, 1.00, and 1.25 mmol/L) of Gd-based contrast agents (Meglumine Gadopentetate (Gd-DTPA) 0.5 mmol/mL, Fujipharma, Japan) were used for the *in vitro* imaging study. We used Gd-DTPA for the phantom study because Gd-DTPA has smaller relaxation rates (R_1) than Gd-EOB-DTPA, which facilitated the adjustment of T_1 values for each phantom. To determine the optimal TI for PSIR, 10 phantoms with T_1 values of 154–1054 ms, as estimated by the standard IR-spin echo (IR-SE) (corresponding to concentrations of 0.10–1.25 mmol/L), were imaged by PSIR with four different TIs (300, 400, 500, and 600 ms). The real and reference images were acquired using exactly the same imaging parameters that were employed for T_1 estimation, which were TR,

2.8 ms; echo time (TE), 1.3 ms; shot interval, 1500 ms; FA, 10°; field of view (FOV), 360×360 mm²; matrix size, 180×144; TFE factor, 28; acquisition duration, 78.4 ms; slice thickness, 10 mm; SENSE factor, 2; k-space reordering, low–high. The signal intensities (SIs) of the phantoms were measured. The contrast of each phantom was calculated by comparing its SI to that of the control phantom with a T_1 of 1054 ms. The control phantom could be regarded as the T_1 value of a liver tumor in the hepatobiliary phase, which was previously reported as the mean T_1 value of liver metastases from various primaries at 20 min after Gd-EOB-DTPA injection (17). The contrast was determined using

$$\text{Contrast} = \frac{|SI \text{ of phantom} - SI \text{ of phantom}(T_1 = 1054 \text{ ms})|}{|SI \text{ of phantom}| + |SI \text{ of phantom}(T_1 = 1054 \text{ ms})|} \quad (4)$$

The phantoms were also imaged using conventional 3D TFE with FA = 15° and 30°. The imaging parameters were TR, 3.0 ms; TE, 1.37 ms; FOV, 360×328 mm²; matrix size, 180×144; TFE factor, 2; slice thickness, 10 mm; SENSE factor, 3; k-space reordering, sequential; fat suppression, spectral attenuated inversion recovery. The SI and contrast of each phantom were also measured in same fashion as described above.

For the T_1 measurements, the SIs of the real and reference images for all 12 phantoms were measured; then, their T_1 were calculated as described above. These T_1 were validated by comparing them to those obtained using two conventional T_1 estimation methods: IR-SE and L-L. The imaging parameters employed in IR-SE were TR, 6000 ms; TE, 6.9 ms; number of TI, 10; FOV, 350×175 mm²; matrix size, 176×176; slice thickness, 10 mm. The SI of each phantom image was measured, and the T_1 were calculated using a two-parameter fitting procedure. The imaging parameters applied in L-L were TR, 12 ms; TE, 2.4 ms; FOV, 420×270 mm²; matrix size, 112×112; slice thickness, 10 mm; TFE factor, 9; FA, 7°; number of phases, 35; SENSE factor, 2. The SI of each phantom image was measured, and the T_1 were calculated using a three-parameter fitting procedure (19). All of the fitting calculations

were performed using spreadsheet software (Microsoft Excel 2016, Microsoft, Redmond, WA, USA).

For statistical analysis, the Pearson correlation coefficient (r) was employed to evaluate the correlations between the T_1 calculated using PSIR and IR-SE, as well as those between the Gd concentrations and R_1 obtained with PSIR, IR-SE, and L-L by using statistical software (GraphPad Prism6.0, GraphPad Software, La Jolla, CA, USA).

In vivo study

The study protocol was approved by the Institutional Review Board of the Kumamoto Medical Center. After written informed consent was obtained, seven healthy volunteers (mean age, 29.6 years) were enrolled. The T_1 -weighted images were obtained using PSIR with the optimal TI that was determined during the phantom study and the TFE (FA = 15° and 30°). The PSIR imaging parameters were TI, 500 ms; TFE factor, 42; acquisition duration, 115.5 ms; slice thickness, 6 mm; number of slabs, 5; SENSE factor, 3; scan time, 100 s (20 s breath-hold per slab × 5 times to cover entire liver); number of slices, 30. The TFE imaging parameters were TFE factor, 31; slice thickness, 3 mm; scan time, 15 s (a single breath-hold); number of slices, 56; and the other imaging parameters were same as those in the phantom study.

Regions of interest (ROIs) were drawn over the liver, spleen, and muscle in each MR image by one investigator (Y.F.) using ImageJ (<http://imagej.nih.gov/ij/>). For liver parenchyma, a circular, 17-mm-diameter ROI was placed in the right lobe in each image. In the same slice, another circular, 17-mm-diameter ROI was placed in the center of the spleen, while a circular, 14-mm-diameter ROI was placed in the erector spine muscle. The liver-to-spleen and liver-to-muscle contrasts were calculated using Eq. 4 and then compared with each sequence. Friedman's test with *post hoc* multiple comparisons (Dunn's procedure)

was used to compare the differences between the PSIR and TFE contrasts. $p < 0.05$ was considered significant. To validate the simultaneous T_1 estimated by PSIR, the T_1 values of the liver-parenchyma, spleen, and muscle that were calculated using PSIR were compared with those estimated by L-L, and r was employed to assess the correlations between the T_1 values acquired from PSIR and L-L by using GraphPad Prism6.0. Moreover, T_1 parametrical maps were generated using image-processing software (MATLAB2015a, Mathworks, Natick, MA, USA) and pixel-by-pixel iteration of the PSIR images.

Results

Phantom study

Figure 2 shows the differences between the T_1 values of the investigated and control phantoms versus the contrast between the examined and control phantoms in each imaging scenario. The image contrasts obtained using PSIR with different TI settings are equivalent when the T_1 difference is large (>500 ms). However, the contrasts of the PSIR results acquired with TI = 300–400 ms are lower than those of the results with TI = 500–600 ms when the T_1 difference is small (200–500 ms). The PSIR images obtained with each TI tested also show contrasts higher than those of the TFE images. The T_1 estimated using PSIR in each TI setting were linearly correlated with those measured using IR-SE (Fig. 3a). However, when TI is low (300 and 400 ms), this linear correlation is weaker in the range with higher T_1 . Thus, the optimal TI for PSIR was determined to be 500–600 ms. The estimated R_1 of the phantoms that were measured using PSIR, IR-SE, and L-L are well correlated with their Gd concentrations. Additionally, the differences among the three methods are negligible except at high Gd concentrations, where more noticeable, though still slight, differences are observable (Fig. 3b). Bland-Altman plots were also examined and showed no systematic variations

between the IR-SE and PSIR results with $TI = 500$ ms and $R_1 < 5.13$ s⁻¹ or between the IR-SE/PSIR and L-L results (Fig. 3c).

In vivo study

In the *in vivo* study results shown in Fig. 4, the PSIR results exhibit liver-to-spleen and liver-to-muscle contrasts that are significantly higher than those of the TFE results. Representative images obtained using each method are presented in Fig. 5. The contrast between the liver and the other organs, such as the spleen and muscles, is more noticeable in the PSIR images than in the TFE images. Representative T_1 maps obtained using PSIR are shown in Fig. 6a. The T_1 values of the liver parenchyma, spleen, and muscle that were estimated using PSIR are clearly correlated with those obtained using L-L (Fig. 6c).

Discussion

We demonstrated the feasibility of using PSIR liver imaging to obtain T_1 contrasts between the liver parenchyma and the other organs higher than those obtainable with conventional methods and to measure the T_1 value of the liver parenchyma precisely and simultaneously. As shown in Fig. 2, the image contrast achieved using PSIR was larger than the contrasts obtained using TFE with $FA = 15^\circ$ and 30° . Furthermore, the T_1 contrast realized by using PSIR is higher than that resulting from using TFE, even when the difference between their T_1 contrasts is only slight. This improvement could result from the fact that an additional IR pulse is applied in PSIR, prior to the TFE. Then, the magnetization in the equilibrium state becomes $-M_0$ due to each IR pulse, and the T_1 relaxation is achieved with time. This indicates that the T_1 contrast would ideally be increased two-fold compared with M_0 (23). Therefore, PSIR can yield a T_1 contrast higher than that obtainable using TFE over a wide range of Gd concentrations. This increased contrast may be advantageous for EOB-MRI

and could enable the detection of liver lesions that exhibit only slight T_1 differences from the liver parenchyma.

The PSIR images obtained in the *in vivo* study exhibited contrasts between the liver and the other organs, such as the spleen and muscle, that were higher than those of the TFE images. These results are consistent with those reported in previous neuroimaging studies in which IR sequences were employed (24, 25). The higher liver-to-muscle contrast obtained using PSIR might indicate that such sequences improve the tumor-to-liver contrast in the hepatobiliary phase of EOB-MRI in patients with severe liver dysfunction. This is because the T_1 of the muscle and liver tumor are equivalent (18), while the T_1 value of the normal liver parenchyma without Gd-EOB-DTPA resemble those of the liver parenchyma with less Gd-EOB-DTPA accumulation due to severe liver dysfunction (20).

In addition, the T_1 estimated using PSIR and IR-SE in the phantom study were highly correlated with one another. Particularly, for $TI > 500$ ms, a strong linear correlation was observed over a wide T_1 range. However, for $TI < 500$ ms, this linear correlation weakened, especially in the high- T_1 range. Therefore, we determined the optimal TI for PSIR to be 500 ms. Since the reference signal was acquired immediately after the first shot interval time and TI, the timing of the second acquisition depended on the setting of TI in the PSIR. Setting TI to be short decreased the reference signal intensity, causing M_E and M_F to be underestimated. As a result, T_1 value was overestimated. If the timing of the second acquisition could be changed manually, TI might not affect the accuracy of the T_1 estimated using PSIR. Furthermore, the R_1 estimated with PSIR and $TI = 500$ ms showed an excellent linear correlation with the Gd concentration and were identical to those obtained using IR-SE and L-L, except at high Gd concentrations, where slight differences were observed among the values determined using these three methods. These deviations may be attributable to the fact that different fitting procedures are used in these methods. However, since the estimated T_1 of

the normal liver parenchyma has been reported to be less than approximately $T_1 = 340$ ms ($R_1 = 3.0$ s⁻¹) in the hepatobiliary phase (20), these deviations observed at high Gd concentrations may not present a critical problem for clinical applications. Therefore, we believe that the T_1 measurement accuracy of PSIR is identical to those of the conventional imaging methods. For the *in vivo* study, PSIR successfully produced a parametric T_1 map covering the entire liver with high resolution, which is difficult to achieve using other conventional methods. This may be useful not only for partial liver function assessment, but also for the differential diagnosis of liver tumors using T_1 (18). Accurate quantification of liver T_1 might also be useful for follow-up examinations after treatment, even with different MR imaging environments.

However, our study has several limitations. First, the sample size was relatively small, the subjects were all healthy volunteers, and Gd-EOB-DTPA was not administered. Although our results imply that PSIR could improve the liver-to-tumor contrast of EOB-MRI especially in the patients with severe liver dysfunction, a clinical study with GD-EOB-DTPA must be performed to verify the utility of PSIR for liver MR imaging. Second, PSIR requires a long acquisition time because reference data must be obtained. More repetitions of multi-slab acquisition and multiple breath holds are needed to cover the entire liver region because the additional IR pulses prolong the total imaging time. By using the respiratory gating technique or higher acceleration imaging technique, shorter acquisition times might be achievable in the future (26, 27).

In conclusion, PSIR improved the T_1 contrast between phantoms with different Gd concentrations, as well as the liver-to-spleen/liver-to-muscle T_1 contrast *in vivo* compared to TFE and simultaneously provided accurate T_1 maps of liver parenchyma. Although a clinical study is necessary to evaluate the clinical utility of PSIR, these results suggest that PSIR may be capable of improving liver MR imaging.

Conflict of interest

The authors declared no potential conflicts of interest with respect of the research, authorship, and/or publication of this article.

Funding

The authors received no financial support for the research, authorship, and/or publication this article.

References

1. Vogl TJ, Kümmel S, Hammerstingl R, et al. Liver tumors: comparison of MR imaging with Gd-EOB-DTPA and Gd-DTPA. *Radiology* 1996; 200: 59–67.
2. Tamada T, Ito K, Yamamoto A, et al. Hypointense hepatocellular nodules on hepatobiliary phase of Gd-EOB-DTPA-enhanced MRI: can increasing the flip angle improve conspicuity of lesions? *J Magn Reson Imaging* 2013; 37: 1093–1099.
3. Kim AY, Kim YK, Lee MW, et al. Detection of hepatocellular carcinoma in gadoxetic acid-enhanced MRI and diffusion-weighted MRI with respect to the severity of liver cirrhosis. *Acta Radiol* 2012; 53: 830–838.
4. Bashir MR, Merkle EM. Improved liver lesion conspicuity by increasing the flip angle during hepatocyte phase MR imaging. *Eur Radiol* 2011; 21: 291–294.
5. Bashir MR, Husarik DB, Ziemlewicz TJ, et al. Liver MRI in the hepatocyte phase with gadolinium-EOB-DTPA: Does increasing the flip angle improve conspicuity and detection rate of hypointense lesions? *J Magn Reson Imaging* 2012; 35: 611–616.
6. Haradome H, Grazioli L, Manea AI K, et al. Gadoxetic acid disodium-enhanced hepatocyte phase MRI: can increasing the flip angle improve focal liver lesion detection? *J Magn Reson Imaging* 2012; 35: 132–139.
7. Geisel D, Lüdemann L, Wagner C, et al. Evaluation of gadolinium-EOB-DTPA uptake after portal vein embolization: value of an increased flip angle. *Acta Radiol* 2014; 55: 149–154.
8. Okada M, Wakayama T, Yada N, et al. Optimal flip angle of Gd-EOB-DTPA-enhanced MRI in patients with hepatocellular carcinoma and liver metastasis. *Abdom Imaging* 2014; 39: 694–701.
9. Verloh N, Haimerl M, Zeman F, et al. Assessing liver function by liver enhancement during the hepatobiliary phase with Gd-EOB-DTPA-enhanced MRI at 3 Tesla. *Eur Radiol* 2014; 24: 1013–1019.
10. Yamada A, Hara T, Li F, et al. Quantitative Evaluation of Liver Function with Use of Gadoxetate Disodium-enhanced MR Imaging. *Radiology* 2011; 260: 727–733.
11. Utsunomiya T, Shimada M, Hanaoka J, et al. Possible utility of MRI using Gd-EOB-DTPA for estimating liver functional reserve. *J Gastroenterol* 2012; 47: 470–476.
12. Zhao X, Huang M, Zhu Q, et al. The relationship between liver function and liver parenchymal contrast enhancement on Gd-BOPTA-enhanced MR imaging in the hepatocyte phase. *Magn Reson Imaging* 2015; 33: 768–773.
13. Saito K, Ledsam J, Sourbron S, et al. Measuring hepatic functional reserve using low temporal resolution Gd-EOB-DTPA dynamic contrast-enhanced MRI: a preliminary

- study comparing galactosyl human serum albumin scintigraphy with indocyanine green retention. *Eur Radiol* 2014; 24: 112–119.
14. Ryeom H-K, Kim S-H, Kim J-Y, et al. Quantitative evaluation of liver function with MRI using Gd-EOB-DTPA. *Korean J Radiol* 2004; 5: 231–239.
 15. Okada M, Murakami T, Yada N, et al. Comparison between T1 relaxation time of Gd-EOB-DTPA-enhanced MRI and liver stiffness measurement of ultrasound elastography in the evaluation of cirrhotic liver. *J Magn Reson Imaging* 2015; 41: 329–338.
 16. Norén B, Forsgren MF, Dahlqvist Leinhard O, et al. Separation of advanced from mild hepatic fibrosis by quantification of the hepatobiliary uptake of Gd-EOB-DTPA. *Eur Radiol* 2013; 23: 174–181.
 17. Goshima S, Kanematsu M, Watanabe H, et al. Gd-EOB-DTPA-enhanced MR imaging: prediction of hepatic fibrosis stages using liver contrast enhancement index and liver-to-spleen volumetric ratio. *J Magn Reson Imaging* 2012; 36: 1148–1153.
 18. Yoshimura N, Saito K, Saguchi T, et al. Distinguishing hepatic hemangiomas from metastatic tumors using T1 mapping on gadoxetic-acid-enhanced MRI. *Magn Reson Imaging* 2013; 31: 23–27.
 19. Deichmann R and Haase A. Quantification of T_1 values by SNAPSHOT-FLASH NMR imaging. *J Magn Reson* 1992; 96: 608–612.
 20. Katsube T, Okada M, Kumano S, et al. Estimation of liver function using T1 mapping on Gd-EOB-DTPA-enhanced magnetic resonance imaging. *Invest Radiol* 2011; 46: 277–283.
 21. Kellman P, Arai AE, McVeigh ER, et al. Phase-sensitive inversion recovery for detecting myocardial infarction using gadolinium-delayed hyperenhancement. *Magn Reson Med* 2002; 47: 372–383.
 22. Warntjes MJB, Kihlberg J, Engvall J. Rapid T1 quantification based on 3D phase sensitive inversion recovery. *BMC Med Imaging* 2010; 10: 19.
 23. Bernstein MA, King KF, Zhou XJ. *Handbook of MRI Pulse Sequences*. Elsevier, 2004.
 24. Poonawalla AH, Hou P, Nelson FA, et al. Cervical spinal cord lesions in multiple sclerosis: T1-weighted inversion-recovery MR imaging with phase-sensitive reconstruction. *Radiology* 2008; 246: 258–264.
 25. Hou P, Hasan KM, Sitton CW, et al. Phase-sensitive T1 inversion recovery imaging: a time-efficient interleaved technique for improved tissue contrast in neuroimaging. *AJNR Am J Neuroradiol* 2005; 26: 1432–1438.

26. Nagle SK, Busse RF, Brau AC, et al. High resolution navigated three-dimensional T₁-weighted hepatobiliary MRI using gadoxetic acid optimized for 1.5 Tesla. *J Magn Reson Imaging* 2012; 36: 890–899.
27. Yu MH, Lee JM, Yoon JH, et al. Clinical application of controlled aliasing in parallel imaging results in a higher acceleration (CAIPIRINHA)-volumetric interpolated breathhold (VIBE) sequence for gadoxetic acid-enhanced liver MR imaging. *J Magn Reson Imaging* 2013; 38: 1020–1026.

Figure legends

Fig. 1.

Schematic of magnetization evolution during 3D acquisition. Horizontal and vertical axes indicate time and M_0 , respectively. Using PSIR, image acquisition was performed twice with same flip angle = 10° after applying IR pulse during single breath holds; real and reference data were obtained. Segmented k-space reordering was set to low-high for both acquisitions. M_0 during data acquisition relaxes in accordance with T_1^* , which is shorter than T_1 , due to RF pulse excitation, while it relaxes in accordance with T_1 during periods without RF pulses.

Fig. 2.

Relationship between difference in T_1 value from that of control phantom ($T_1 = 1054$ ms) and contrast between examined and control phantoms in each imaging scenario. PSIR contrasts with different TI settings are equivalent when T_1 difference is large (>500 ms). However, PSIR contrast with TI = 300–400 ms is lower than if TI = 500–600 ms in smaller T_1 difference range (200–500 ms). PSIR with any TI tested in this study yielded higher contrasts than those of TFE.

Fig. 3.

(a) Comparison of T_1 estimated using PSIR with different TI against T_1 estimated using IR-SE. Graphs show linear correlations between two methods with any TI settings ($r = 0.997$, 0.999 , 0.999 , and 0.999 for TI = 300, 400, 500, and 600 ms, respectively), but slight discordances are observable in higher T_1 range (>1500 ms), especially with TI = 300 ms and 400 ms. (b) Comparison of estimated relaxation rate $R_1 (=1/T_1)$ measured using PSIR, IR-SE, and L-L and actual Gd concentration. Excellent linear correlations are observable in all methods ($r = 0.999$), but slight discordances are identifiable in high-Gd-concentration

phantoms. (c) Bland-Altman plots of IR-SE vs. PSIR (TI = 500 ms), IR-SE vs. L-L, and L-L vs. PSIR (TI = 500 ms).

Fig. 4.

(a) Liver-to-muscle and (b) liver-to-spleen contrasts in healthy subjects. PSIR results show contrasts significantly higher than those of TFE results (PSIR: 1.16 ± 0.14 , TFE with FA = 15° : 0.30 ± 0.12 , TFE with FA = 30° : 0.44 ± 0.23 for liver-to-spleen contrast, and PSIR: 1.30 ± 0.26 , TFE with FA = 15° : 0.22 ± 0.03 , TFE with FA = 30° : 0.22 ± 0.05 for liver-to-muscle contrast).

Fig. 5.

Representative *in vivo* images of PSIR and TFE with FA = 15° and 30° .

Fig. 6.

Representative (a) gray-scale T_1 maps obtained using PSIR. Average T_1 values and standard deviations of liver parenchyma, spleen, and muscle estimated by PSIR were 738.4 ± 36.5 , 1286.1 ± 137.0 , and 1085.4 ± 23.4 ms. (b) Scatter plots of T_1 values of liver parenchyma, spleen, and muscle measured using PSIR and L-L show high linear correlations ($r = 0.979$). Estimated slope coefficient and intercept (\pm standard error) of linear regression line were determined to be 1.288 ± 0.062 and -152.4 ± 58.54 .

Figure 1

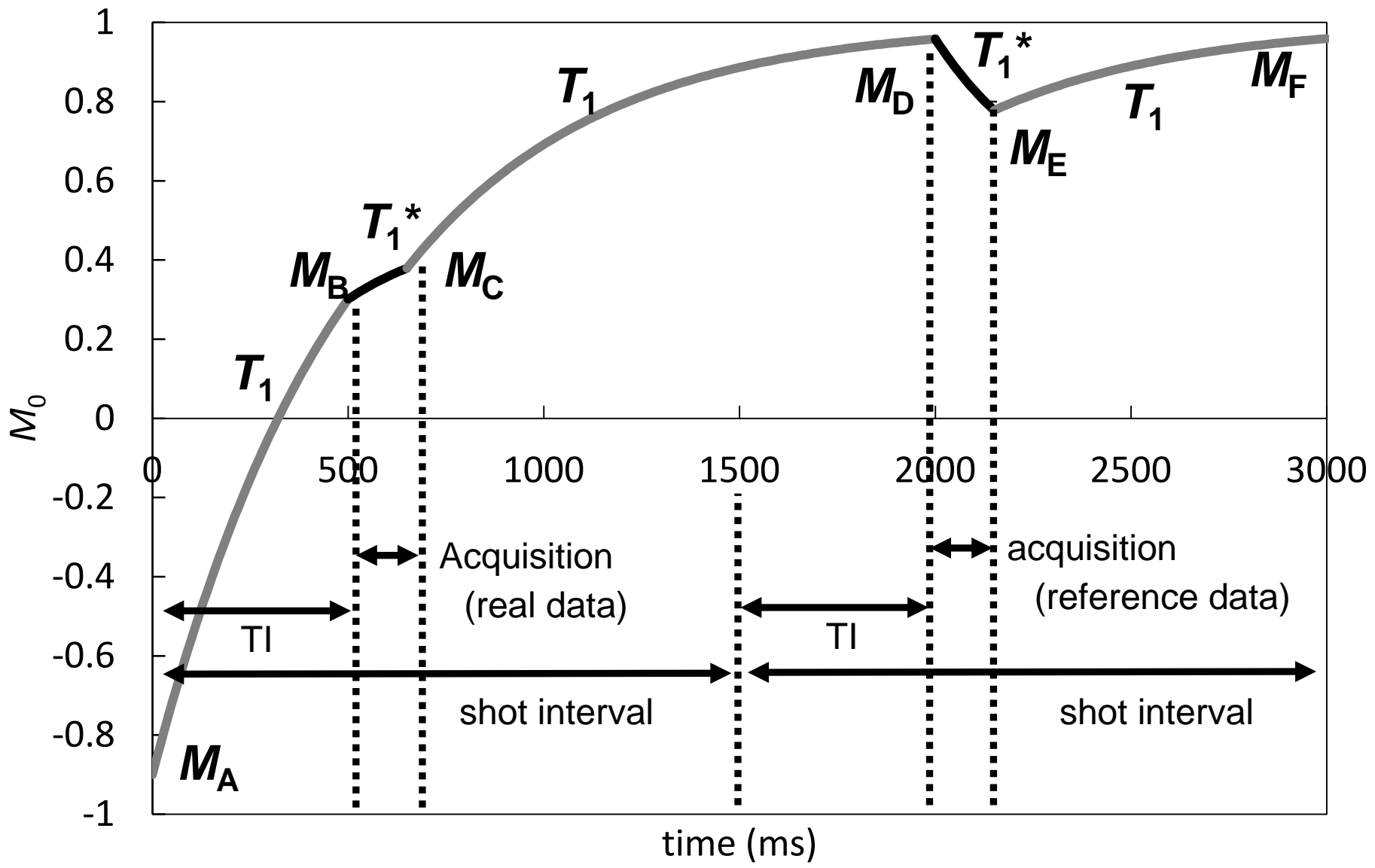


Figure 2

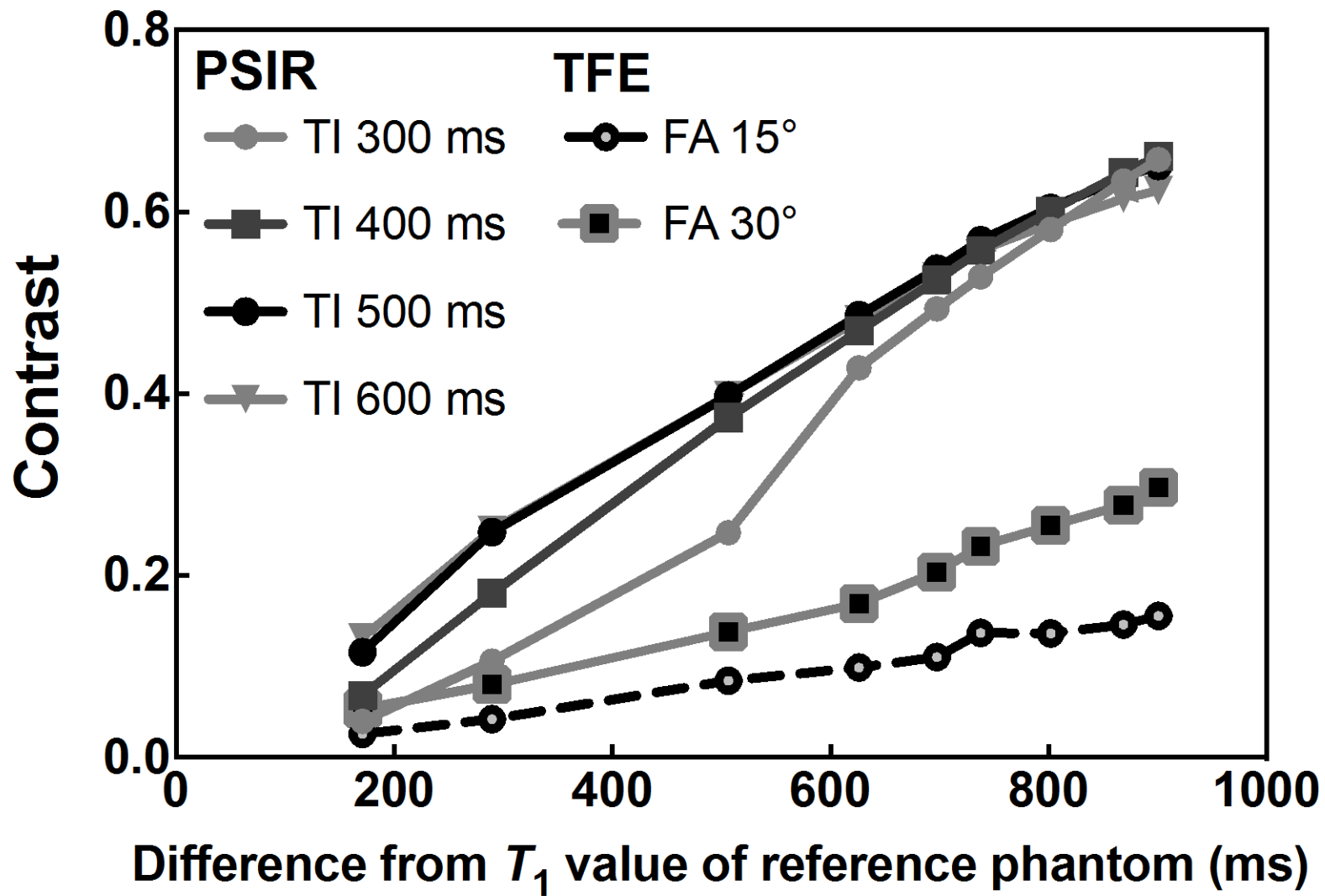


Figure 3

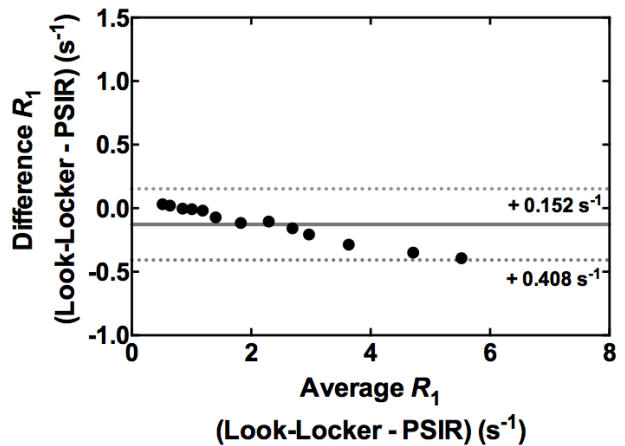
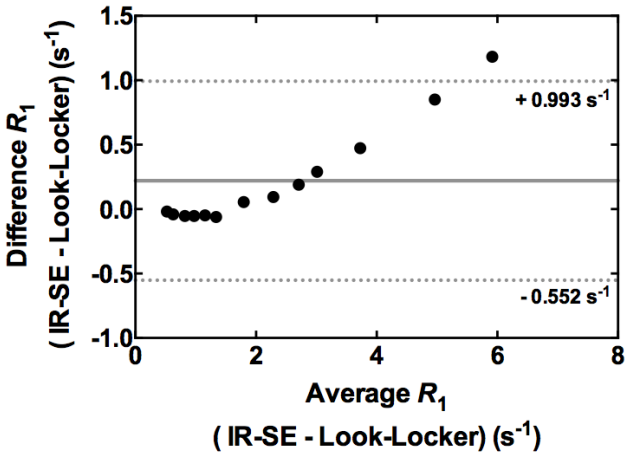
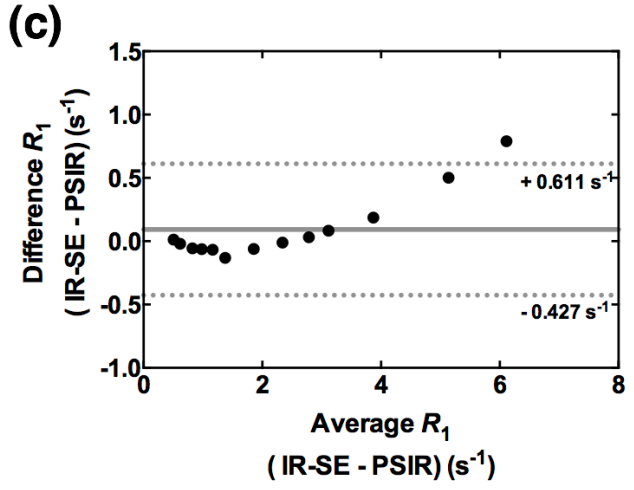
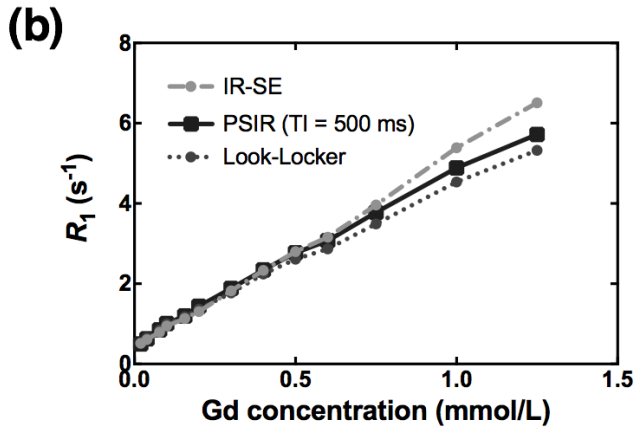
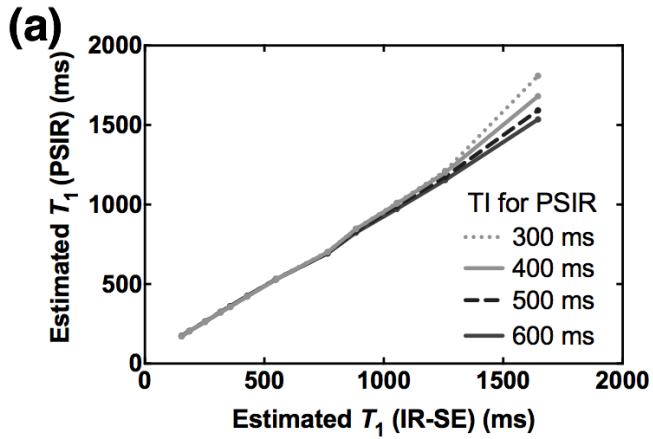


Figure 4

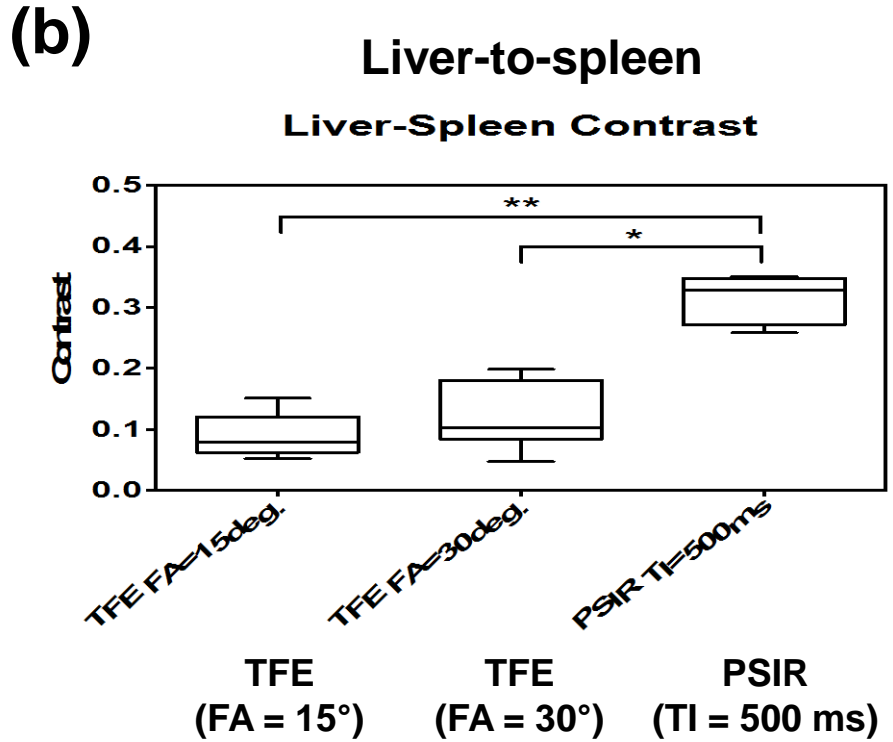
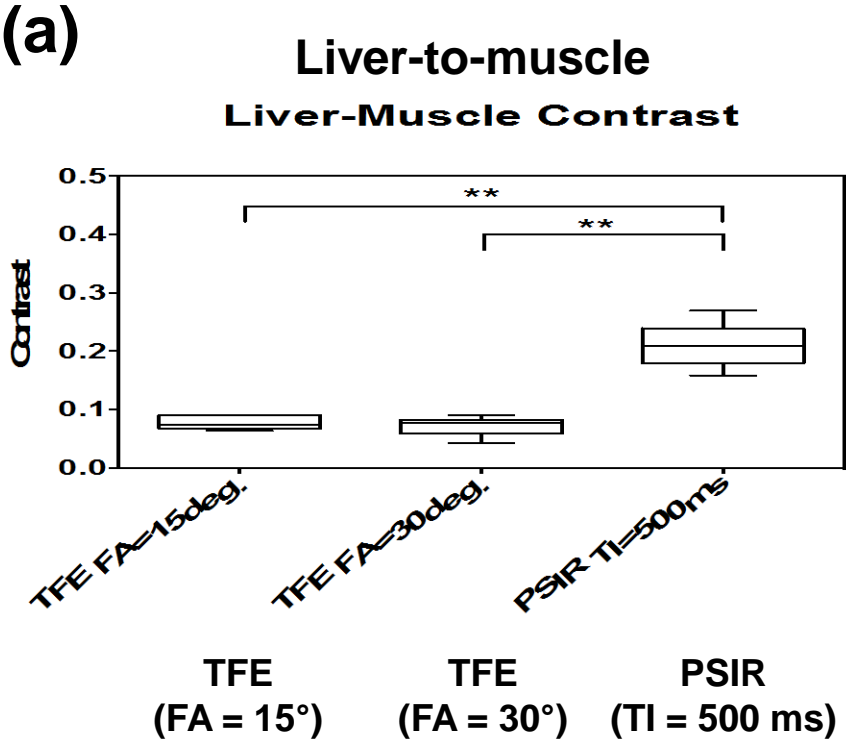
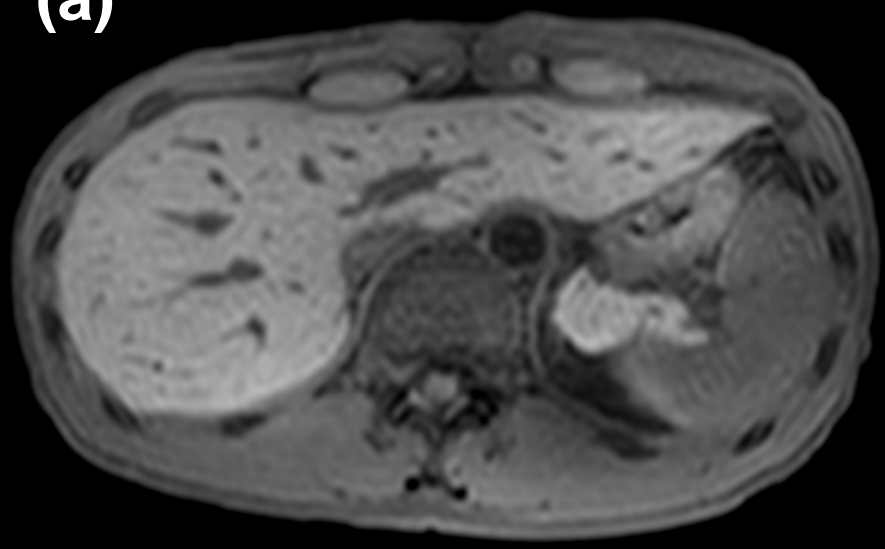
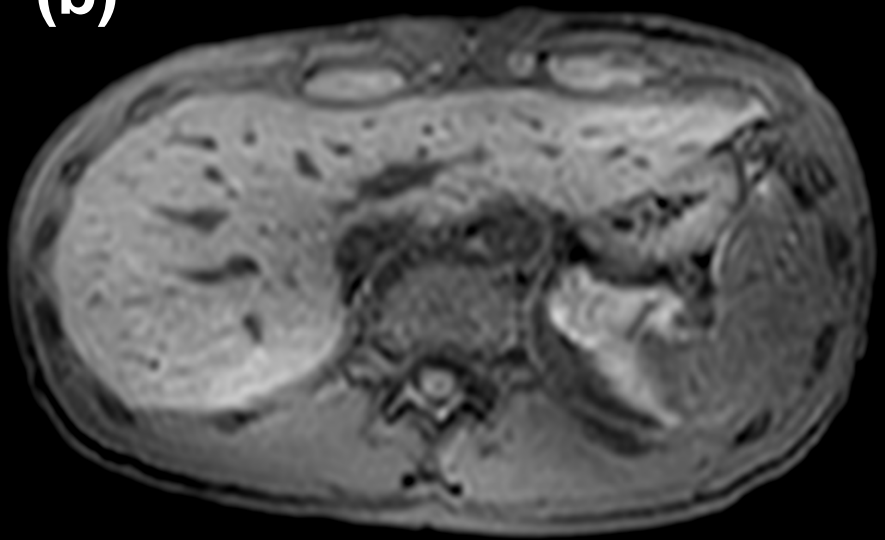


Figure 5

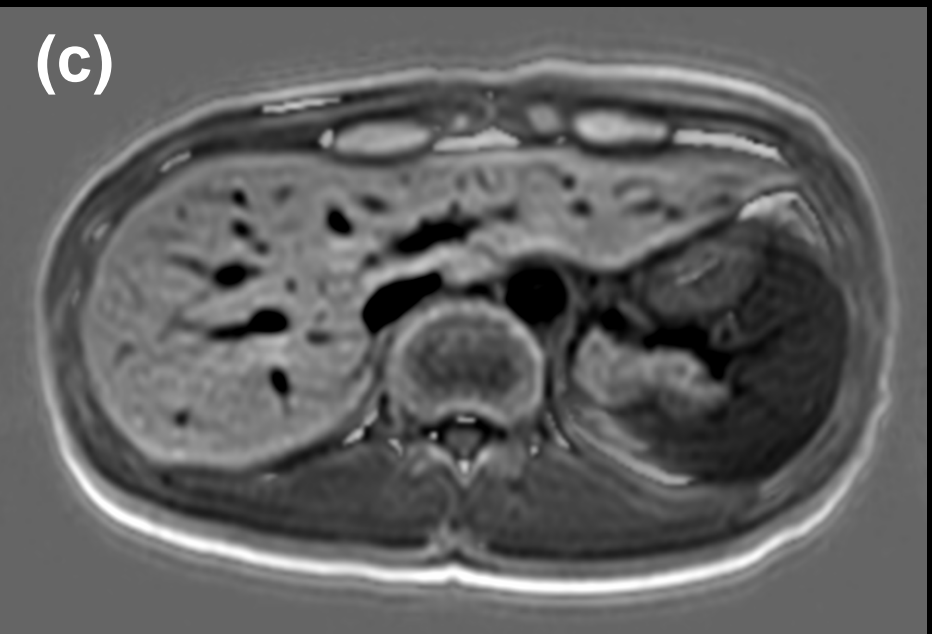
(a)



(b)



(c)



**TFE
(FA = 15°)**

PSIR

**TFE
(FA = 30°)**

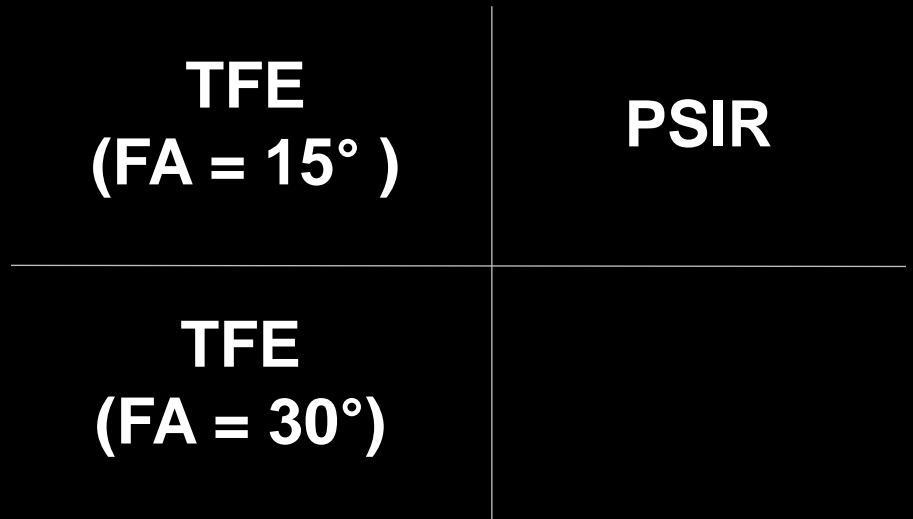
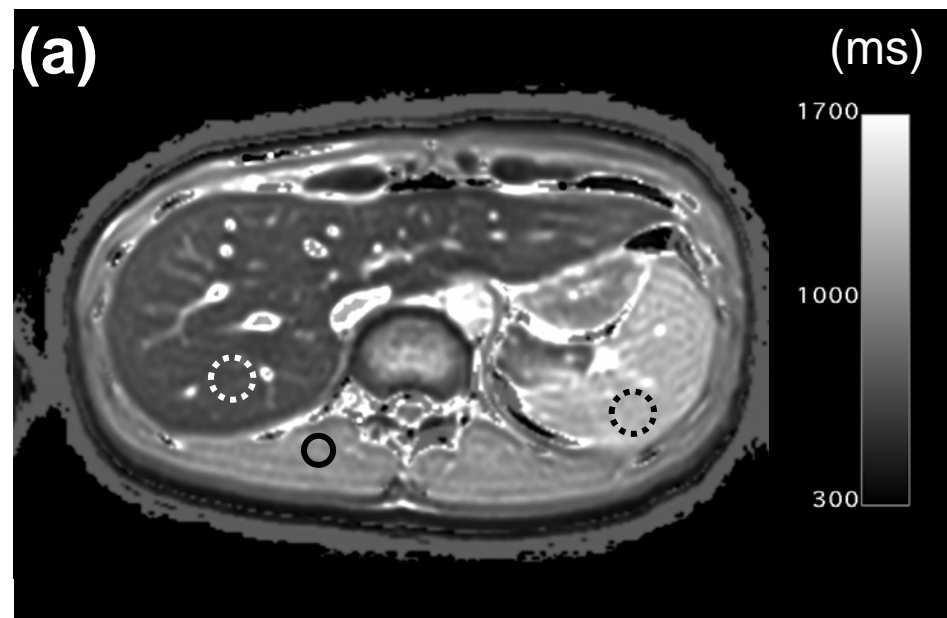


Figure 6



(b) in vivo study T1 value

